

Combining Density Functional Theory and Green’s Function Theory: Range-Separated, Non-local, Dynamic, and Orbital-Dependent Hybrid Functional

Alexei A. Kananenka¹ and Dominika Zgid¹

¹*Department of Chemistry, University of Michigan, Ann Arbor, Michigan 48109, United States**

We present a rigorous framework that combines single-particle Green’s function theory with density functional theory based on a separation of electron-electron interactions into short-range and long-range components. Short-range contributions to the total energy and exchange-correlation potential are provided by a density functional approximation, while the long-range contribution is calculated using an explicit many-body Green’s function method. Such a hybrid results in a non-local, dynamic, and orbital-dependent exchange-correlation functional of a single-particle Green’s function. In particular, we present a range-separated hybrid functional called srSVWN5—lrGF2 which combines the local-density approximation and the second-order Green’s function theory. We illustrate that similarly to density functional approximations the new functional is weakly basis-set dependent. Furthermore, it offers an improved description of the short-range dynamical correlation. The many-body contribution to the functional allows us to mitigate the many-electron self-interaction error present in most of density functional approximations and provides a better description of molecular properties. Additionally, the new functional can be used to scale down the self-energy and, therefore, introduce an additional sparsity to the self-energy matrix that in the future can be exploited in calculations for large molecules or periodic systems.

I. INTRODUCTION

Kohn–Sham density functional theory (DFT)^{1–3} has become a method of choice for unraveling the ground state properties of mostly single reference molecular and condensed matter systems. Its popularity is due to an attractive compromise between the accuracy and computational cost, provided by numerous approximations to the exchange-correlation functional. The best approximate functionals offer a decent description of the short-range dynamical correlation which justifies their use for near-equilibrium geometries. Another attractive feature of density functionals is their weak dependence on the one-electron basis set. Despite their large success, however, local and semilocal density functionals fail to describe a number of important properties, for example, charge transfer excitations⁴, dynamical long-range correlations important in weak van der Waals complexes bound by London dispersion forces⁵, and Rydberg excitation energies⁶. The reason for this failure is well understood and is rooting in a wrong asymptotic behavior of the exchange-correlation potential which in turn is a consequence of a self-interaction error⁷.

Many-body wave-function methods such as the Møller–Plesset perturbation theory (MP2)⁸, coupled cluster (CC)⁹ or multiconfigurational self-consistent field (MC-SCF)¹⁰ approaches are capable of providing a correct description when density functionals fail. However, for these *ab-initio* methods, in addition to a steep computational cost and long configuration expansion of the wave function also large basis sets are required to describe the dynamical correlation accurately and reach an agreement with experiments. These features make the application of *ab-initio* methods to very large systems quite challenging and much larger system sizes can be reached when density functional approximations are used.

In recent years, there has been a substantial progress in the development of density functionals that mix both the standard local or semilocal density functional approximation with the wave-function theory. The mixing is done rigorously by separating the two-electron interaction operator into short-range and long-range components^{11–13} resulting in so-called range-separated hybrid functionals¹⁴. They are meant to combine the best features of the respective approaches. The least computationally expensive range-separated hybrid functional is obtained when a non-local Hartree–Fock-type exchange is introduced to replace the long-range exchange density functional^{15–19}. Such functionals were proved successful in a partial correction of the long-range behavior of the exchange-correlation potential^{17,20}. However, they are also known to perform worse than standard density functionals in some cases^{15,21}.

The combination of explicit many-body wave-function methods with the density-functional theory by means of range separation has been previously quite extensively explored. Long-range MP2^{22–25}, second-order *n*-electron valence state perturbation theory (NEVPT2)²⁶, coupled cluster (CCSD(T))²⁷, random-phase approximation (RPA)^{28–30}, configuration interaction (CI)^{12,31}, MC-SCF^{32,33}, and the density-matrix-functional theory^{34,35} have been combined with short-range local and semilocal density functionals^{13,16,27,36,37}. These range-separated functionals were successfully applied to weakly interacting molecular systems^{22,27,29,30,38–41}. In comparison to corresponding standard many-body wave-function approaches, the range-separated functionals have additional advantages such as a rapid convergence with respect to the basis set size^{22,24,27–30,42–46} and smaller basis-set superposition errors. In these approaches, the long-range correlation energy is usually added as a post-SCF correction to the total energy from a range-separated calculation without the long-range correlation functional.

Therefore, they do not yield the exact energy even with the exact short-range exchange-correlation functional, for example see ref 30.

Since the srSVWN5—lrGF2 functional introduced in this work combines both the density functional theory and the Green’s function theory, we aim to provide a self-contained and detailed description that can be useful to both these communities. Therefore, to bring the readers to a common ground, we found it helpful to list some key theory concepts from both communities.

Finite-temperature single-particle Green’s function methods have been long known in the context of condensed matter physics^{47–49} and now are making inroads into quantum chemistry^{50–54}. These methods are rigorous and offer several advantages. The single-particle Green’s function formalism is based entirely on one-electron operators avoiding the necessity of dealing with wave functions. A single-particle Green’s function determines the expectation value of single-particle operators, the two-electron correlation energy, and provides access to the spectral density, ionization potentials and electron affinities.

In this work, we present a rigorous self-consistent framework combining a short-range density functional approximation with a long-range single-particle Green’s function method. As a specific example, we implemented and benchmarked the short-range local density approximation (LDA)^{55,56} with the second-order Green’s function theory (GF2)^{50,57,58}. To further motivate this work, it is worth to briefly list differences between the method presented here and the already existing plethora of range-separated hybrid functionals. Most methods that have been previously applied to the long-range interactions were not self-consistent. In contrast to non-self-consistent methods, which are starting point dependent, the approach presented here, irrespective of the initial guess, recovers the exact total electronic energy provided that both the exact short-range exchange-correlation functional and the exact long-range Green’s function method are used. An iterative nature of GF2 results in multiple implications. The overall accuracy of GF2 for weakly correlated systems is close to that of MP2 or CCSD, however, unlike these two approaches, GF2 does not display divergences for strongly correlated systems⁵⁰. GF2 is a one-electron self-interaction free method, while methods such as RPA contain a significant one-electron self-interaction error⁵⁹. Furthermore, a Matsubara axis GF2 formalism is explicitly temperature-dependent.

The range-separated hybrid functional presented here also shares some commonalities with other combinations of DFT with Green’s function methods. For example, the LDA+DMFT⁶⁰ method that combines LDA with the dynamical mean-field theory (DMFT)⁶¹ is often used in solid state calculations of strongly correlated systems. However, LDA+DMFT is known to suffer from a so-called double counting problem^{60,62}, where some electronic correlations are accounted for by both

LDA and DMFT. In the LDA+DMFT method, these two sources of electronic correlations cannot be rigorously separated^{60,63,64}. We would like to stress that the double counting problem does not appear in the framework presented here since the exact separation of the electron-electron interaction into long- and short-range components is used.

Range-separated hybrid functionals employ a single range separation parameter controlling the spatial extent of the short-range contribution. The optimal value of this system-dependent parameter^{65–67} can be determined either by empirical fitting against available experimental data^{15,18,68,69} or in an *ab-initio* fashion in a self-consistent procedure^{14,68}. In our current work, we have adopted the latter view and applied the optimal tuning strategy based on calculations of ionization potentials to find optimal values of the range separation parameter for several atoms and molecules. Additionally, we have also investigated the two-electron self-interaction error, basis set dependence, dynamical correlation as well as the implications of the hybrid functional presented here for the Green’s function based embedding methods and periodic calculations.

II. THEORY

The exact electronic ground state energy of a system of N interacting electrons in the presence of external potential $v(\mathbf{r})$ (e.g., the potential of the nuclei) can be obtained by a two-step minimization of the following functional⁷⁰

$$E_{\text{tot}}[\rho] = \min_{\rho \rightarrow N} \left\{ F[\rho] + \int d\mathbf{r} v(\mathbf{r}) \rho(\mathbf{r}) \right\}, \quad (1)$$

where $\rho(\mathbf{r})$ is an electron density and $F[\rho]$ is the universal functional of the electron density that is defined as

$$F[\rho] = \min_{\Psi \rightarrow \rho} \langle \Psi | \hat{T} + \hat{V}_{ee} | \Psi \rangle, \quad (2)$$

where $\hat{T} = -\frac{1}{2} \sum_i^N \nabla_i^2$ is the kinetic energy operator, $\hat{V}_{ee} = \frac{1}{2} \sum_{i \neq j}^N \hat{v}_{ee}(r_{ij})$ is the electron-electron interaction operator, $r_{ij} = |\mathbf{r}_i - \mathbf{r}_j|$ and \mathbf{r}_i is the coordinate vector of electron i . The minimization is first carried out over all normalized antisymmetric wave functions Ψ that produce a given density $\rho(\mathbf{r})$, and then over all densities yielding N -electrons. The existence and uniqueness of the universal functional $F[\rho]$ is guaranteed by Hohenberg and Kohn theorem¹. Regrettably, an explicit variation of eq 1 has not become practical since no exact form of the universal functional is available and due to its absence all practical applications are based on the Kohn–Sham scheme². This procedure uses an approximation to the exchange-correlation part of the universal functional. One of the most successful approaches taken along this way is the combination of two (or more) density functional approximations into one so-called hybrid exchange-correlation functional using the adiabatic connection theorem^{71–74}.

Range-separated density functional approximations belong to a particular class of hybrid functionals¹⁴. The essence of range-separated hybrid functionals lies in the decomposition of the Coulomb electron-electron interaction operator into a sum of short-range and long-range counterparts^{11,12,75},

$$\begin{aligned} \frac{1}{r_{ij}} &= \hat{v}_{ee}^{sr,\lambda}(r_{ij}) + \hat{v}_{ee}^{lr,\lambda}(r_{ij}) \\ &= \underbrace{\frac{1-f(\lambda r_{ij})}{r_{ij}}}_{\text{short-range}} + \underbrace{\frac{f(\lambda r_{ij})}{r_{ij}}}_{\text{long-range}}, \end{aligned} \quad (3)$$

with the parameter λ controlling the range separation. The function $f(\lambda r)$ satisfies the following properties $f(\lambda r \rightarrow \infty) = 1$ and $f(\lambda r \rightarrow 0) = 0$. From a physical and computational standpoint the standard error function $f(\lambda r) = \text{erf}(\lambda r)$ is one of the most convenient choices. The decomposition in eq 4 is exact and presents a convenient starting point for developing range-separated hybrid functionals by mixing a short-range density functional approximation with a long-range method. The universal functional from eq 2 is partitioned accordingly¹³

$$F[\rho] = \min_{\Psi \rightarrow \rho} \langle \Psi^\lambda | \hat{T} + \hat{V}_{ee}^{lr,\lambda} | \Psi^\lambda \rangle + E_{\text{H}}^{sr,\lambda}[\rho] + E_{\text{xc}}^{sr,\lambda}[\rho], \quad (4)$$

$$\begin{aligned} E_{\text{tot}}[\rho] &= \min_{\rho \rightarrow N} \left\{ \min_{G \rightarrow \rho} \{T[G] + E_{ee}^{lr,\lambda}[G]\} + E_{\text{H}}^{sr,\lambda}[\rho] + E_{\text{xc}}^{sr,\lambda}[\rho] + \int d\mathbf{r} v(\mathbf{r})\rho(\mathbf{r}) \right\} \\ &= \min_{G \rightarrow N} \left\{ T[G] + E_{ee}^{lr,\lambda}[G] + E_{\text{H}}^{sr,\lambda}[\rho] + E_{\text{xc}}^{sr,\lambda}[\rho] + \int d\mathbf{r} v(\mathbf{r})\rho(\mathbf{r}) \right\}, \end{aligned} \quad (7)$$

where the electron density $\rho(\mathbf{r})$ is calculated from the Green's function $G \rightarrow \rho$. Note that the single-particle Green's function minimizing eq 8 yields both the exact electron density ρ and proper total number of electrons N . Therefore, we can define the total energy functional as

$$E_{\text{tot}}[G] = T[G] + E_{ee}^{lr,\lambda}[G] + E_{\text{H}}^{sr,\lambda}[G] + E_{\text{xc}}^{sr,\lambda}[\rho] + \int d\mathbf{r} v(\mathbf{r})\rho(\mathbf{r}). \quad (8)$$

The long-range electron-electron interaction energy can be decomposed into the Hartree long-range energy and the long-range exchange-correlation energy

$$E_{ee}^{lr,\lambda}[G] = E_{\text{H}}^{lr,\lambda}[G] + E_{\text{xc}}^{lr,\lambda}[G]. \quad (9)$$

The short-range and long-range Hartree energies can be folded into one term describing the all-range Hartree energy $E_{\text{H}}[\rho]$. This leads to the following expression for the energy functional defined in eq 9

$$E_{\text{tot}}[G] = T[G] + E_{\text{H}}[\rho] + E_{\text{xc}}^{sr,\lambda}[G] + E_{\text{xc}}^{lr,\lambda}[G] + \int d\mathbf{r} v(\mathbf{r})\rho(\mathbf{r}). \quad (10)$$

where the first term defines the long-range universal functional $F^{lr,\lambda}[\rho]$, the second term $E_{\text{H}}^{sr,\lambda}[\rho]$ is the short-range Hartree functional, and the third term $E_{\text{xc}}^{sr,\lambda}[\rho]$ is the short-range exchange-correlation functional. The total energy from eq 1, therefore, can be rewritten as

$$E_{\text{tot}}[\rho] = \min_{\rho \rightarrow N} \left\{ F^{lr,\lambda}[\rho] + E_{\text{H}}^{sr,\lambda}[\rho] + E_{\text{xc}}^{sr,\lambda}[\rho] + \int d\mathbf{r} v(\mathbf{r})\rho(\mathbf{r}) \right\}. \quad (5)$$

To formulate a self-consistent theory including a long-range exchange and correlation energies coming from a Green's function method, we redefine the long-range functional $F^{lr,\lambda}[\rho]$ as the following functional of a single-particle Green's function G

$$F^{lr,\lambda}[\rho] = \min_{G \rightarrow \rho} \{T[G] + E_{ee}^{lr,\lambda}[G]\}. \quad (6)$$

Here, $T[G]$ is the kinetic energy functional and $E_{ee}^{lr,\lambda}[G]$ is the long-range interaction functional of a single-particle Green's function. The search is performed over all single-particle Green's functions yielding a given density $\rho(\mathbf{r})$. Consequently, we can write the ground state electronic energy as a functional of a single-particle Green's function

This energy functional (that depends on a Green's function) provides an exact decomposition of the total energy into short-range and long-range components. In particular, there is no double counting of correlation effects. The minimization of this functional with respect to a single-particle Green's function yields the ground state energy. It should be noted that with the exact long-range Green's function method and exact short-range density functional the minimization of eq 11 will produce the exact ground state electronic energy for all possible range separation parameters λ .

In practical calculations of realistic systems, both the short-range and long-range methods must be approximated. When employed in a range-separated framework, the standard density functional approximations are modified to describe short-range interactions. The short-range exchange-correlation energy is calculated as

$$E_{\text{xc}}^{sr,\lambda} = \int d\mathbf{r} \rho(\mathbf{r}) \epsilon_{\text{xc}}^{sr,\lambda}(\rho), \quad (11)$$

where $\epsilon_{\text{xc}}^{sr,\lambda}(\rho)$ is the short-range exchange-correlation energy density. The short-range LDA exchange energy den-

sity $\epsilon_{x,\sigma}^{sr,\lambda}(\rho)$ can be derived from the exchange hole of the homogeneous electron gas interacting with a short-range electron-electron interaction potential³⁶. Its functional

$$\epsilon_{x,\sigma}^{sr,\lambda}(\rho) = -\frac{1}{2} \left(\frac{3}{4\pi} \right)^{1/3} \rho_\sigma^{1/3}(\mathbf{r}) \left(1 - \frac{8}{3} a_\sigma \left[\sqrt{\pi} \operatorname{erf} \left(\frac{1}{2a_\sigma} \right) + (2a_\sigma - 4a_\sigma^3) \exp \left(-\frac{1}{4a_\sigma^2} \right) - 3a_\sigma + 4a_\sigma^3 \right] \right), \quad (12)$$

where $a_\sigma = \lambda/(2k_{F,\sigma})$, k_σ is the Fermi momentum given by $k_{F,\sigma} = (6\pi^2\rho_\sigma)^{1/3}$ and $\sigma = \alpha, \beta$ is the spin index. This approximation reduces to the standard LDA exchange energy density at $\lambda = 0$ and has a correct asymptotic expansion for $\lambda \rightarrow \infty$ ¹³. Thus, it provides an interpolation between LDA and the correct limit as $\lambda \rightarrow \infty$. LDA was shown to be exact at the short-range⁷⁶ and, when combined with the many-body perturbation theory, such a hybrid method is expected to give an improved description of the dynamical correlation both in comparison to LDA and the perturbation theory. Consequently, in this case LDA is used to recover a fraction of the dynamical correlation that is missing in the finite order of perturbation theory. In subsection IV B, we provide results supporting this discussion by investigating dynamical correlation in diatomic molecules.

In order to calculate the short-range correlation energy density $\epsilon_c^{sr,\lambda}(\rho)$, we adopted a scheme based on the following rational approximant^{36,37}

$$\epsilon_c^{sr,\lambda}(r_s) = \frac{\epsilon_c(r_s)}{1 + c_1(r_s)\lambda + c_2(r_s)\lambda^2}, \quad (13)$$

where $\epsilon_c(r_s)$ is the correlation energy density for the standard Coulomb interactions ($\lambda = 0$) evaluated for the Wigner-Seitz radius $r_s(\rho) = (3/(4\pi\rho))^{1/3}$ with $\rho(\mathbf{r}) = \rho_\alpha(\mathbf{r}) + \rho_\beta(\mathbf{r})$. Equation 13 provides a way to interpolate between $\lambda = 0$ and $\lambda \rightarrow \infty$ limits and is applicable not only for the interpolation of the correlation energy density but can also be used for the exchange energy density¹³. Particular forms of $c_1(r_s)$ and $c_2(r_s)$ depend on the quantity interpolated. In this work, we used $c_1(r_s)$ and $c_2(r_s)$ determined by Toulouse *et. al.* by analytical parameterization of the long-range correlation energy density from CCD and Fermi-hypernetted-chain calculations of the uniform electron gas³⁶. The short-range correlation energy density was then calculated as a difference between all-range and long-range correlation energy densities. In this work, we have investigated two local density approximations for the correlation energy: Vosko–Wilk–Nusair (VWN5) functional (“form V” parametrization in ref 56) as well as the Perdew and Wang (PW92) functional⁷⁷. PW92 uses the same spin-interpolation formula as the VWN functional but employs different expressions for the paramagnetic correlation energy density and the ferromagnetic correction to it. After performing several test calculations, we noticed that total energies from the short-range VWN5 functional were within 1 kcal-mol⁻¹

of those of the short-range PW92 functional. Consequently, we proceeded by using short-range VWN5 functional and all results reported in this work were obtained with it.

Having discussed theoretical background behind short-range density functionals and our specific choices, we now turn to the discussion of the long-range electron-electron interaction energy. The long-range exchange energy is defined exactly in terms of the Fock exchange integral as

$$E_x^{lr,\lambda} = -\frac{1}{2} \sum_\sigma \int d\mathbf{r} \int d\mathbf{r}' \frac{|\gamma_\sigma(\mathbf{r}, \mathbf{r}')|^2 \operatorname{erf}(\lambda|\mathbf{r} - \mathbf{r}'|)}{|\mathbf{r} - \mathbf{r}'|}, \quad (14)$$

where $\gamma_\sigma(\mathbf{r}, \mathbf{r}')$ is the one-electron reduced density matrix. Note that the incorporation of the screening provided by the error function leads to a faster decaying long-range exchange contribution and, especially for metallic systems, can result in reducing the computational cost¹⁶.

In this work, we propose to calculate the long-range correlation energy using single-particle Green’s function methods. In a Green’s function formalism, it is possible to correct a zeroth order Green’s function $\mathcal{G}(\omega)$ (which in certain cases can be a non-interacting Green’s function) using the Dyson equation⁴⁷

$$\mathbf{G}_\sigma(\omega) = [\mathcal{G}_\sigma(\omega)^{-1} - \Sigma_\sigma(\omega)]^{-1}, \quad (15)$$

where $\Sigma_\sigma(\omega)$ is the self-energy of the system. The self-energy is an effective single-particle potential that incorporates all many-body effects present in the system. At this point, a connection to the density functional theory can be made. The frequency-dependent self-energy $\Sigma(\omega)$ shares some similarities with the exchange-correlation potential of DFT $v_{xc}(\rho)$ since $v_{xc}(\rho)$ also connects interacting and non-interacting systems. However, we stress that unlike $v_{xc}(\rho)$ in Kohn–Sham DFT, the self-energy is a dynamic, nonlocal and orbital-dependent quantity. This implies that a treatment of such potentials is beyond the Kohn–Sham scheme and it requires the so-called generalized Kohn–Sham framework (GKS)⁷⁸.

Calculating either the exact exchange-correlation potential or the exact self-energy is an inconceivably complicated task. Fortunately, a hierarchy of systematically improvable approximations to the self-energy is provided by the many-body perturbation theory^{48,79}. Examples of such approaches include GF2, GW^{80,81}, and FLEX^{82,83} approximations.

Since both the long-range exchange (eq 14) and the long-range correlation energy (eq 16) should be calculated self-consistently with their short-range counterparts, it is important that such a self-consistent evaluation can be carried out easily. Moreover, for Green's function methods, only fully iterative schemes respect the conservation laws and ensure that quantities obtained by a thermodynamic or coupling constant integration from non-interacting limits are consistent^{84,85}

This is why in our work, we did not employ any real axis single-particle Green's functions $\mathbf{G}(\omega)$ that are rational functions in the complex plane. The rational structure of $\mathbf{G}(\omega)$ implies the existence of poles, for which, iterative algorithms require pole shifting techniques^{86–88}. Consequently, the real axis Green's functions methods are known to present problems during self-consistent schemes.

We are employing an imaginary axis, single-particle Green's function $\mathbf{G}(i\omega_n)$ that is a smooth function of the imaginary argument $i\omega_n$ and is used to describe single-particle properties of a statistical ensemble. Due to the smooth structure, $\mathbf{G}(i\omega_n)$ is a convenient quantity for self-consistent calculations. The imaginary frequency (Matsubara) Green's function $\mathbf{G}(i\omega_n)$ is expressed on a grid of imaginary frequencies located at $i\omega_n = i(2n + 1)\pi/\beta$ ⁸⁹, where $n = 0, 1, 2, \dots$, $\beta = 1/(k_B T)$ is the inverse temperature, k_B is the Boltzmann constant and T is the physical temperature. Providing that the imaginary frequency self-energy and Green's function were self-consistently determined⁴⁸, the long-range correlation energy can be calculated using the Galitskii–Migdal formula⁹⁰

$$E_c^{lr,\lambda} = k_B T \sum_n \text{Re} \left[\text{Tr} \left[\mathbf{G}_\alpha^\lambda(i\omega_n) \Sigma_\alpha^{lr,\lambda}(i\omega_n) + \mathbf{G}_\beta^\lambda(i\omega_n) \Sigma_\beta^{lr,\lambda}(i\omega_n) \right] \right]. \quad (16)$$

We have presented equations for calculating long-range exchange (eq 14) and long-range correlation energies (eq 16), however, as we mentioned before, is important that they are calculated self-consistently with their short-range counterparts.

Here, we outline an algorithm that allows us to perform such a self-consistent evaluation. It should be noted that the formalism presented in this work is general and not limited to a specific choice of the Green's function method and the density functional approximation.

1. The calculation begins with an initial guess for the density matrix \mathbf{P} . For all calculations presented in this work, the Hartree–Fock density matrix was used for this purpose. The method is, however, reference-independent and different choices of the initial density matrix are possible and the same converged solution should be reached irrespective of the starting point.
2. The electron density is calculated using a finite set

of L basis functions $\{\phi_i(\mathbf{r})\}$

$$\rho_\sigma(\mathbf{r}) = \sum_{ij}^L P_{ij}^\sigma \phi_i(\mathbf{r}) \phi_j(\mathbf{r}). \quad (17)$$

3. The density matrix is used to calculate the all-range Hartree contribution to the Fock matrix according to

$$J_{ij} = \sum_{kl} \left(P_{kl}^\alpha + P_{kl}^\beta \right) v_{ijkl}, \quad (18)$$

where v_{ijkl} are unscreened two-electron integrals

$$v_{ijkl} = \int d\mathbf{r} \int d\mathbf{r}' \frac{\phi_i^*(\mathbf{r}) \phi_j(\mathbf{r}) \phi_k^*(\mathbf{r}') \phi_l(\mathbf{r}')}{|\mathbf{r} - \mathbf{r}'|}. \quad (19)$$

4. The short-range exchange-correlation energy is calculated using eqs 11, 12, 13 and the corresponding contributions to the Fock matrix are given by

$$\begin{aligned} [V_{x,\sigma}^{sr,\lambda}]_{ij} &= \int d\mathbf{r} v_{x,\sigma}^{sr,\lambda}(\rho) \phi_i(\mathbf{r}) \phi_j(\mathbf{r}), \\ [V_{c,\sigma}^{sr,\lambda}]_{ij} &= \int d\mathbf{r} v_c^{sr,\lambda}(\rho) \phi_i(\mathbf{r}) \phi_j(\mathbf{r}), \end{aligned} \quad (20)$$

where the short-range exchange $v_{x,\sigma}^{sr,\lambda}(\rho)$ and short-range correlation $v_c^{sr,\lambda}(\rho)$ potentials are functional derivatives of short-range exchange and short-range correlation functionals with respect to the electron density: $v_{x,\sigma}^{sr,\lambda}(\rho) = \delta E_x^{sr,\lambda}[\rho] / \delta \rho_\sigma(\mathbf{r})$ and $v_c^{sr,\lambda}(\rho) = \delta E_c^{sr,\lambda}[\rho] / \delta \rho_\sigma(\mathbf{r})$, respectively.

5. Each of the spin components of the non-interacting Matsubara Green's function is then built according to

$$\mathcal{G}_\sigma(i\omega_n) = [(i\omega_n + \mu_\sigma) \mathbf{S} - \mathbf{F}_\sigma]^{-1}, \quad (21)$$

where μ_σ is the chemical potential, \mathbf{S} is the overlap matrix and \mathbf{F}_σ is the Fock matrix containing all-range Hartree and short-range exchange-correlation parts

$$\mathbf{F}_\sigma = \mathbf{H}^{\text{core}} + \mathbf{J} + \mathbf{V}_{x,\sigma}^{sr,\lambda} + \mathbf{V}_{c,\sigma}^{sr,\lambda}, \quad (22)$$

where \mathbf{H}^{core} is the core Hamiltonian matrix

$$H_{ij}^{\text{core}} = \int d\mathbf{r} \phi_i^*(\mathbf{r}) \left(-\frac{1}{2} \nabla_{\mathbf{r}}^2 + v(\mathbf{r}) \right) \phi_j(\mathbf{r}) \quad (23)$$

and $v(\mathbf{r})$ is the external potential.

6. The Green's function from step 5 is then used to generate either the long-range self-energy $\mathcal{G}(i\omega_n) \rightarrow \Sigma^{lr,\lambda}(i\omega_n)$ or directly the correlated Green's function depending on a particular Green's function method used. Both quantities are needed later and the Dyson eq 15 is used to obtain one from the other.

7. The long-range exchange contribution to the Fock matrix is calculated according to

$$K_{ij,\sigma}^{lr,\lambda} = - \sum_{kl} P_{kl}^{\sigma} v_{ilkj}^{lr,\lambda}. \quad (24)$$

The interacting Green's function at this point reads as

$$\mathbf{G}_{\sigma}^{\lambda}(i\omega_n) = [(i\omega_n + \mu_{\sigma})\mathbf{S} - \mathbf{F}_{\sigma} - \Sigma_{\sigma}^{lr,\lambda}(i\omega_n)]^{-1}, \quad (25)$$

where the Fock matrix has now both terms coming from the density functional and the Green's function method

$$\mathbf{F}_{\sigma} = \mathbf{H}^{\text{core}} + \mathbf{J} + \mathbf{V}_{x,\sigma}^{sr,\lambda} + \mathbf{V}_{c,\sigma}^{sr,\lambda} + \mathbf{K}_{\sigma}^{lr,\lambda}. \quad (26)$$

The long-range self-energy $\Sigma_{\sigma}^{lr,\lambda}(i\omega_n)$ describes the dynamical (frequency-dependent) long-range correlation.

8. The long-range correlation energy is calculated using the correlated Green's function $\mathbf{G}_{\sigma}^{\lambda}(i\omega_n)$ and the long-range self-energy $\Sigma_{\sigma}^{lr,\lambda}(i\omega_n)$ according to eq 16.
9. The total electronic energy is calculated according to

$$E_{\text{tot}} = \frac{1}{2} \text{Tr} [(\mathbf{H}^{\text{core}} + \mathbf{f}_{\alpha})\mathbf{P}_{\alpha} + (\mathbf{H}^{\text{core}} + \mathbf{f}_{\beta})\mathbf{P}_{\beta}] + E_{xc}^{sr,\lambda} + E_x^{lr,\lambda} + E_c^{lr,\lambda}, \quad (27)$$

where

$$\mathbf{f}_{\sigma} = \mathbf{H}^{\text{core}} + \mathbf{J} + \mathbf{K}_{\sigma}^{lr,\lambda}. \quad (28)$$

10. The interacting Green's function is then used to update the density matrix

$$\mathbf{P}_{\sigma} = \frac{1}{\beta} \sum_n e^{i\omega_n 0^+} \mathbf{G}_{\sigma}^{\lambda}(i\omega_n). \quad (29)$$

11. The total electronic energy, density matrix, and Green's function are checked for convergence and, if necessary, a new iteration is started by sending updated density matrix to step 2.

The above algorithmic construction is in principle general and can be used in finite-temperature calculations to evaluate the grand potential as

$$\Omega = \Phi - \text{Tr}(\log \mathbf{G}^{-1}) - \text{Tr}(\Sigma \mathbf{G}), \quad (30)$$

where Φ is the Luttinger–Ward (LW)⁹¹ functional that is a scalar functional of a renormalized Green's function and is defined as the sum of all closed, connected and fully dressed skeleton diagrams. The general $\Phi[\mathbf{G}]$ functional has the following form

$$\Phi[\mathbf{G}] = E_{\text{H}}[\mathbf{G}] + E_{\text{x}}[\mathbf{G}] + E[\mathbf{G}] \quad (31)$$



FIG. 1. A formal definition of the Luttinger–Ward functional as a skeleton diagrammatic expansion, shown here for the second-order theory. Black solid lines represent Green's functions and red wiggly lines denote electron-electron interactions (two-electron integrals).

where $E[\mathbf{G}]$ is the correlation energy coming from frequency dependent $\Sigma(i\omega_n)$ and $\mathbf{G}(i\omega_n)$. Since $\delta\Phi/\delta G_{ij}(i\omega_n) = \Sigma_{ij}(i\omega_n)$, we obtain the following expression for the self-energy

$$\Sigma_{\sigma} = \mathbf{J} + \mathbf{K}_{\sigma} + \Sigma_{\sigma}(i\omega_n). \quad (32)$$

Application of the decomposition from eq 4 can be understood as a splitting of interaction lines for every diagram leading to the following expression for the self-energy

$$\Sigma_{\sigma} = \mathbf{J} + \mathbf{K}_{\sigma}^{sr,\lambda} + \mathbf{K}_{\sigma}^{lr,\lambda} + \Sigma_{\sigma}^{sr,\lambda}(i\omega_n) + \Sigma_{\sigma}^{lr,\lambda}(i\omega_n). \quad (33)$$

Finally, when a hybrid functional with DFT is considered, short-range exchange and short-range correlation self-energies are approximated by static (frequency-independent) corresponding potentials from the density functional approximation: $\mathbf{K}_{\sigma}^{sr,\lambda} \rightarrow \mathbf{V}_{x,\sigma}^{sr,\lambda}$ and $\Sigma_{\sigma}^{sr,\lambda}(i\omega_n) \rightarrow \mathbf{V}_{c,\sigma}^{sr,\lambda}$ resulting in the following expression for the self-energy

$$\Sigma_{\sigma} = \mathbf{J} + \mathbf{V}_{x,\sigma}^{sr,\lambda} + \mathbf{V}_{c,\sigma}^{sr,\lambda} + \mathbf{K}_{\sigma}^{lr,\lambda} + \Sigma_{\sigma}^{lr,\lambda}(i\omega_n), \quad (34)$$

which enters the expression for the correlated Green's function shown earlier in eqs 25 and 26. While in principle the presented formalism that merges DFT with Green's function theory is temperature dependent and completely general, in our work, we use two simplifications. First, all practical calculations are currently limited to the $T = 0$ case due to lack of reliable explicit finite-temperature density functional approximations. Second, in our work, for simplicity, we have employed the finite-temperature, self-consistent, second-order Green's function theory (GF2) for evaluating $\Sigma_{\sigma}^{lr,\lambda}(i\omega_n)$. Consequently, in equations 32 to 34, we use $\Sigma_{\sigma}(i\omega_n) = \Sigma_{2,\sigma}(i\omega_n)$, $\Sigma_{\sigma}^{sr,\lambda}(i\omega_n) = \Sigma_{2,\sigma}^{sr,\lambda}(i\omega_n)$, and $\Sigma_{\sigma}^{lr,\lambda}(i\omega_n) = \Sigma_{2,\sigma}^{lr,\lambda}(i\omega_n)$. The corresponding second-order Feynman diagrams for Φ are shown in Figure 1. Since for the reasons discussed above, the DFT part of calculations is carried out at $T = 0$, we evaluate the GF2 self-energy and Green's function for large β , corresponding to $T \rightarrow 0$. For gapped systems, these calculations are equivalent to the $T = 0$ regime.

One of the key advantages of range-separated hybrid functionals stems from the fact that partitioning in eq 4 is chosen such that a singularity is only present in the short-range operator at electron-electron coalescence, while the long-range contribution is smooth. The absence of the

singularity in the long-range part has significant consequences. Most importantly, a correlated method applied to the long-range electron-electron interactions will not need to represent a cusp using a finite set of one-electron basis functions, thus avoiding basis sets containing functions with very high angular momentum. In contrast to most electron correlation methods, density functionals are weakly basis-set dependent. Therefore, range-separated hybrid functionals usually exhibit faster convergence of the correlation and total energies with the size of the basis set. In subsection IV A, we illustrate that this indeed the case for the functional presented in this work.

In practical applications, a value of the range separation parameter λ has to be specified before a calculation is carried out. It is important that this value is chosen such that the respective approximations are evaluated within a regime that is optimal for their performance¹⁴. The simplest estimation of an optimal value of λ is based on a local approximation³¹ $\lambda(\rho) = r_s(\rho)^{-1}$. The physical motivation behind this value is related to the fact that an electron on average occupies the sphere with boundaries defined by the Wigner–Seitz radius (also known as a characteristic length of the exchange). Therefore, electrons begin to enter an occupation sphere of the other electrons when $\lambda(\rho) \geq r_s(\rho)^{-1}$.

More sophisticated ways to find an optimal value of λ are based on the first-principles approaches and amount to finding λ satisfying some relationships that an exact theory should obey. For instance, a vertical ionization potential (IP) of a molecule containing N electrons is defined as

$$\text{IP}_{E(N)}^{E(N-1)} = E_{\text{tot}}(N-1) - E_{\text{tot}}(N), \quad (35)$$

where $E_{\text{tot}}(N)$ is the total ground state energy of a cation and $E_{\text{tot}}(N)$ is the total ground state energy of a neutral molecule. In an exact theory, $\text{IP}_{E(N)}^{E(N-1)}$ should exactly agree with the IP calculated from the real frequency Green’s function of N -electron (neutral) system $\mathbf{G}_N(\omega)$. The general idea of the IP tuning approach is therefore to require that IP from $\mathbf{G}_N(\omega)$ is as close as possible to IP calculated from total energies of $N-1$ and N electron systems. Therefore, an optimal value of λ can be found by a minimization of the following bijective function

$$\mathcal{T}_N(\lambda) = \left| \text{IP} [\mathbf{G}_N^\lambda(\omega)] - \text{IP}_{E(N)}^{E(N-1)} \right|, \quad (36)$$

where $\text{IP} [\mathbf{G}_N^\lambda(\omega)]$ is the ionization potential calculated from the real frequency Green’s function for a given value of λ . The minimum of $\mathcal{T}_N(\lambda)$ defines an optimal λ for which the ionization potential from a Green’s function calculated for N -electron system is the closest to the ionization potential calculated from total energies of $N-1$ and N electron systems. It is important to emphasize that such tuning procedure does not require any empirical input.

Several methods of calculating IP from a single-particle Matsubara Green’s function of an N -electron system

including the extended Koopmans theorem (EKT)^{92–95} have been proposed. In this work, we adopted the following approach. First, the converged Fock matrix \mathbf{F} coming from the imaginary axis GF2 calculation is transformed to the canonical representation \mathcal{E} . Then the real frequency Green’s function is constructed according to

$$\mathbf{G}(\omega) = [\omega + \mu - \mathcal{E}]^{-1}, \quad (37)$$

where ω is the real frequency grid point. Then the second-order self-energy on the real frequency axis is calculated as follows⁹⁶

$$\begin{aligned} \Sigma_{ij}(\omega) = & \frac{1}{2} \sum_{ars} \frac{\langle rs||ia\rangle\langle ja||rs\rangle}{\omega + \mathcal{E}_a - \mathcal{E}_r - \mathcal{E}_s} \\ & + \frac{1}{2} \sum_{abr} \frac{\langle ab||ir\rangle\langle jr||ab\rangle}{\omega + \mathcal{E}_r - \mathcal{E}_a - \mathcal{E}_b}, \end{aligned} \quad (38)$$

where i, j denote both occupied and virtual spin orbitals, a, b denote the occupied spin orbitals only, and r, s label virtual spin orbitals, $\langle rs||ia\rangle$ are the antisymmetrized two-electron integrals. Occupied and virtual orbitals are defined with respect to the Hartree–Fock determinant. The self-energy is then used to construct an updated real frequency Green’s function according to

$$\mathbf{G}(\omega) = [\omega + \mu - \mathcal{E} - \Sigma(\omega)]^{-1}. \quad (39)$$

The spectral function $\mathbf{A}(\omega)$ is then evaluated using

$$\mathbf{A}(\omega) = -\frac{1}{\pi} \text{Im} \mathbf{G}(\omega). \quad (40)$$

All peaks of $\mathbf{A}(\omega)$ were shifted by the chemical potential μ and IP was set to the closest to $\omega = 0$ peak $\tilde{\omega}$ from ω^- side

$$\text{IP} [\mathbf{G}_N^\lambda(\omega)] = -(\tilde{\omega} + \mu). \quad (41)$$

Results of the IP-tuning approach described above are illustrated in subsection IV C.

Another constraint that an exact electronic structure theory should comply with is based on the energy of fractional electron systems. It is well-known that the total electronic energy should vary linearly in the fractional electron occupancy between integer electron numbers^{97–99}. Inexact methods satisfy this condition only approximately. To the extent that a method deviates from this condition such a method possesses the many-electron self-interaction error. We have investigated this condition on the example of a two-electron system. Results are presented and discussed in subsection IV D.

III. COMPUTATIONAL DETAILS

In this work, we present the range-separated hybrid functional srSVWN5—lrGF2 that combines the SVWN5 density functional with the self-consistent second-order perturbative many-body Green’s function method (GF2). In GF2, the long-range second-order self-energy is calculated in the imaginary time domain according to⁵⁴

$$\begin{aligned}
[\Sigma_{\alpha}^{lr,\lambda}(\tau)]_{ij} &= - \sum_{klmnpq} [G_{\alpha}^{\lambda}(\tau)]_{kl} [G_{\alpha}^{\lambda}(\tau)]_{mn} [G_{\alpha}^{\lambda}(-\tau)]_{pq} v_{ikmq}^{lr,\lambda} (v_{ljpn}^{lr,\lambda} - v_{pjln}^{lr,\lambda}) \\
&\quad - [G_{\alpha}^{\lambda}(\tau)]_{mn} [G_{\beta}^{\lambda}(\tau)]_{kl} [G_{\beta}^{\lambda}(-\tau)]_{pq} v_{ikmq}^{lr,\lambda} v_{ljpn}^{lr,\lambda}, \\
[\Sigma_{\beta}^{lr,\lambda}(\tau)]_{ij} &= - \sum_{klmnpq} [G_{\beta}^{\lambda}(\tau)]_{kl} [G_{\beta}^{\lambda}(\tau)]_{mn} [G_{\beta}^{\lambda}(-\tau)]_{pq} v_{ikmq}^{lr,\lambda} (v_{ljpn}^{lr,\lambda} - v_{pjln}^{lr,\lambda}) \\
&\quad - [G_{\beta}^{\lambda}(\tau)]_{mn} [G_{\alpha}^{\lambda}(\tau)]_{kl} [G_{\alpha}^{\lambda}(-\tau)]_{pq} v_{ikmq}^{lr,\lambda} v_{ljpn}^{lr,\lambda},
\end{aligned} \tag{42}$$

where $G_{kl}^{\lambda}(\tau)$ is the imaginary time Green's function. The algorithm outlined above has been implemented using a locally modified version of the DALTON¹⁰⁰ program for the calculation of long-range two-electron integrals and the short-range SVWN5 exchange-correlation energy and exchange-correlation potential. An in-house GF2 code⁵⁰ was used to perform the self-consistent procedure and to calculate the long-range second-order self-energy. The imaginary time Green's function and self-energy that were optimized for realistic systems were evaluated using the Legendre representation¹⁰¹ and a cubic spline interpolation algorithm¹⁰² was employed to optimize imaginary-frequency quantities. The convergence of the total energy with respect to the size of the Legendre expansion, imaginary time and imaginary frequency grids was verified. Total electronic energies were converged to $5 \cdot 10^{-6}$ au. The inverse temperature was set to $\beta = 100$ au, corresponding to a physical temperature below the excitation energy necessary to occupy the lowest unoccupied level of all systems considered in this work. Results of standard methods: SVWN5, CCSD(T) and FCI, reported in this work, were obtained with GAUSSIAN 09¹⁰³ program.

IV. RESULTS AND DISCUSSION

In this section, we present and analyze numerical results of the application of the srSVWN5—lrGF2 functional to concepts discussed above.

A. Basis set convergence

In this section, for a series of aug-cc-pVXZ augmented correlation-consistent polarization Dunning basis sets^{104–106}, we investigated the convergence of the srSVWN5—lrGF2 total energy as a function of the range separation parameter λ for three systems: He and Mg atoms as well as H₂ molecule at the equilibrium distance $R(\text{H-H}) = 1.4$ au. We studied the convergence of the total energy with respect to the cardinal number X , corresponding to the highest angular momentum in a given basis set \mathcal{L} (note, that for He, $X = \mathcal{L} - 1$). The following values of X were used: $X \in \{D, T, Q, 5\}$ for He and $X \in \{D, T, Q\}$ for H₂ and Mg. Relative to the total energy, obtained for a basis set with $X=5$ for He and

$X=4$ for H₂ and Mg, the total electronic energies of the srSVWN5—lrGF2 functional are plotted in Figure 2. In Figure 2, SVWN5 energies, corresponding to orange lines with triangles, confirm that density functional approximations converge very rapidly with respect to the basis set size. GF2 energies, illustrated by gray lines with diamonds, result in the slowest convergence for every system studied in this work. Any mixture of SVWN5 and GF2 leads to an improved convergence when compared to GF2. For $\lambda < 1$, srSVWN5—lrGF2 converges as fast as SVWN5 for all the systems considered here. For values of $\lambda > 1$, for both H₂ molecule and Mg atom, the convergence of the srSVWN5—lrGF2 functional is much slower than that one of the parent SVWN5 functional. Filled area shown in every plot corresponds to a difference of 1 kcal·mol⁻¹ from the largest basis set used for the system. For all three systems, SVWN5 calculations converged within 1 kcal·mol⁻¹ away from the largest basis set for cc-pVTZ ($X=3$) basis set. For the same basis set, the GF2 energy became almost converged only for H₂ molecule. In Figure 2, for each of the cases analyzed, we also show the largest λ for which the total energy for the cc-pVTZ basis set is 1 kcal·mol⁻¹ away from the energy in the largest basis set used in that system. It corresponds to $\lambda = 5$, $\lambda = 4$ and $\lambda = 0.5$ for He, H₂ and Mg respectively.

Similarly to wave-function methods, pure Green's function methods converge fairly slowly with respect to the basis set size. By using the density functional method to describe short-range interactions a faster convergence with respect to the basis set size is achieved.

B. Potential energy surface of diatomic molecules

The accuracy of popular density functionals around equilibrium geometries stems from a satisfactory description of the short-range dynamical correlation. In this section, we illustrate the dynamical correlation in the srSVWN5—lrGF2 functional by analyzing dissociation curves of diatomic molecules.

First, for the H₂ molecule, we looked at absolute values of the total electronic energy near the equilibrium geometry. We performed spin-restricted total energy calculations using the srSVWN5—lrGF2 functional for different values of the range separation parameter λ scanning over values of interatomic distances around the equilibrium

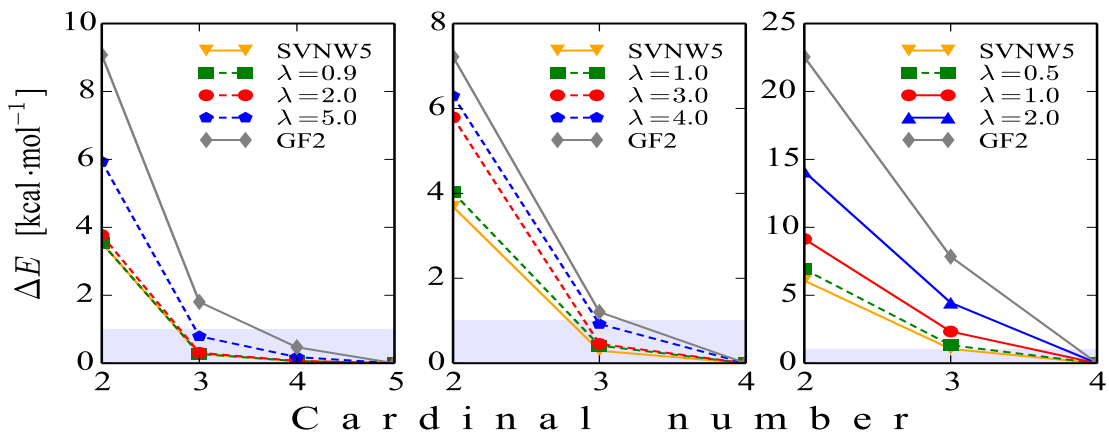


FIG. 2. Basis set convergence as a function of the range separation parameter λ . $\Delta E = |E_{\text{aug-cc-pVYZ}} - E_{\text{aug-cc-pVXZ}}|$ is plotted on the y-axis, while the cardinal number X is plotted on the x-axis. ΔE is given in $\text{kcal}\cdot\text{mol}^{-1}$. The shaded area shown in every plot corresponds to $1 \text{ kcal}\cdot\text{mol}^{-1}$. *Left panel:* Results for the He atom with $X \in \{D, T, Q, 5\}$, $Y = 5$. *Middle panel:* Results for the H_2 molecule at the equilibrium bond length $R(\text{H-H})=1.4 \text{ au}$, with $X \in \{D, T, Q\}$, $Y = 4$. *Right panel:* Results for the Mg atom with $X \in \{D, T, Q\}$, $Y = 4$.

geometry using the cc-pVQZ¹⁰⁴ basis set. The dissociation curve is illustrated in Figure 3. Full Configuration Interaction (FCI) energies are also included and shown for comparison. It is clear that GF2 produces energies that are much closer to FCI than SVWN5. This suggests that GF2 recovers the dynamical correlation better than SVWN5. However, obviously due to a finite order truncation, GF2 does not recover all of the dynamical correlation. GF2, SVWN5, and srSVWN5—lrGF2 tend to be inaccurate far away from equilibrium. This is not surprising since all these methods are not well-suited for systems with a significant strong correlation. As the contribution from GF2 increases (orange line \rightarrow green line \rightarrow cyan line, etc), the total energy gradually approaches the FCI energy and when $\lambda \in [0.7, 0.8]$ the total energy becomes almost stationary with respect to changes in λ . For example, $E(\lambda=0.8) - E(\lambda=0.7) = 0.1 \text{ kcal}\cdot\text{mol}^{-1}$. In particular, $\lambda = 0.7$ corresponds to the best match of the dynamical correlation coming from two respective approaches and produces an equilibrium distance energy which is only $1.7 \text{ kcal}\cdot\text{mol}^{-1}$ away from FCI. For the same internuclear distance, SVWN5 and GF2 errors are $23.1 \text{ kcal}\cdot\text{mol}^{-1}$ and $4.5 \text{ kcal}\cdot\text{mol}^{-1}$, respectively. Overall we conclude that the short-range SVWN5 functional is efficient in adding the missing dynamical correlation to GF2.

The second case we considered was the dissociation of the HF molecule. Rather than looking at the absolute values of the electronic energy, here we focus on the electronic energies relative to the minimum on the dissociation curve. These energies are responsible for the shape of the dissociation curve. The reference energies are provided by CCSD(T)^{9,107} method. The cc-pVQZ basis set was used in all calculations. The results are illustrated in Figure 4. It should be noted that the shape of the GF2 dissociation curve is in a very good agreement with that of CCSD(T), while the SVWN5 energy grows too

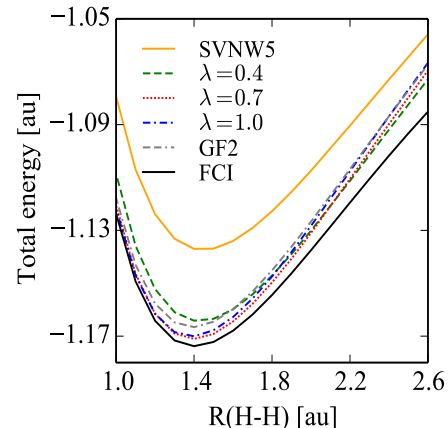


FIG. 3. A dissociation curve of the H_2 molecule calculated using the srSVWN5—lrGF2 functional for different values of λ . The SVWN5, GF2, and FCI results are shown for comparison. All calculations employed the cc-pVQZ basis set.

slow with the increasing internuclear separation beyond the equilibrium distance. Mixing GF2 and SVWN5 for small λ up to $\lambda = 0.3 - 0.4$ fixes this behavior and produces the shape approaching the CCSD(T) quality. As λ increases past $\lambda = 0.4$, the energy as a function of the internuclear separation starts to grow too fast. Mixing in a larger fraction of GF2 turns this behavior around and for $\lambda > 1$, srSVWN5—lrGF2 energies start to slowly approach GF2 energies. For internuclear distances up to $R(\text{H-F})=2.3 \text{ au}$, $\lambda = 0.5$ produces relative energies closely matching those of GF2 and CCSD(T) methods. We conclude that the srSVWN5—lrGF2 functional is able to reproduce correctly the shape of the dissociation curve near the equilibrium geometry. The srSVWN5—

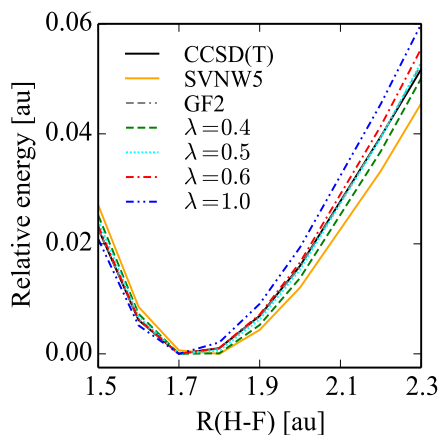


FIG. 4. A dissociation curve of the HF molecule calculated using the srSVWN5—lrGF2 functional for different values of λ . The SVWN5, GF2 and CCSD(T) results are shown for comparison. All calculations employed the cc-pVQZ basis set.

lrGF2 functional does not improve upon GF2, since GF2 being an *ab-initio*, perturbative method already correctly describes the dynamical correlations in the HF molecule. Nonetheless, an apparent improvement comes from the fact that with the srSVWN5—lrGF2 functional these energies can be reached using basis sets with a lower angular momentum when compared to standard GF2, as illustrated in the previous subsection IV A.

C. IP tuning of range-separation parameter λ

Following the prescription given in Section II, we have employed an IP-based tuning approach to find optimal values of the range separation parameter λ for seven closed-shell atoms: He, Be, Ne, Mg, Ca, Ar, and Kr, as well as fifteen closed-shell molecules: H_2CO , CH_4 , NH_3 , N_2 , Li_2 , CO_2 , CO , LiH , CH_3OH , H_2O_2 , N_2H_4 , H_2S , PH_3 , Na_2 , and HCN . Experimental geometries were taken from ref 108. The cc-pVTZ^{104,106,109–111} basis set was used for calculations of both atoms and molecules present in this test set. For the cc-pVTZ and larger basis sets, the value of λ remained constant indicating that it is converged with respect to the basis set size.

To find an optimal value of the range separation parameter for each system in the test set, a series of calculations were performed for $\lambda \in [0.1, 1.5]$ with the step-size set to $\Delta\lambda = 0.1$. In most cases, the \mathcal{T}_N norm as a function of λ was found to have one pronounced minimum that was taken as an optimal λ . For illustration purposes, we show $\mathcal{T}_N(\lambda)$ norm for LiH molecule and Mg atom in Figure 5. In the case of Mg atom, a very small discrepancy between two ways of calculating IP was found for $\lambda = 0.6$ with the error $\mathcal{T}_N \approx 7 \cdot 10^{-4}$ while for LiH molecule the smallest difference between IP $[\mathbf{G}_N^\lambda(\omega)]$ and $\text{IP}_{E(N-1)}^{E(N)}$ turned out to be larger and equal to $\mathcal{T}_N \approx 0.011$

corresponding to the optimal value of $\lambda = 0.2$.

Note that if smaller differences are desired, then a further fine-tuning of λ can be performed by using a root-finding algorithm such as bisection¹¹². In this work, we adopted a commonly used approach and narrowed the optimal value of λ down to only one decimal point. In a similar way, optimal values of the range separation parameter λ were obtained for all systems in this test set.

To examine how accurately IPs can be calculated based on such an IP-tuning approach, we used the optimally tuned srSVWN5—lrGF2 functional to calculate IPs and compared them with IPs calculated using standard SVWN5 and GF2 methods, as well as experiment. The experimental vertical IPs were taken from ref 108. For consistency IPs for GF2, srSVWN5—lrGF2 with the optimal λ , and SVWN5 were calculated according to eq 35 and listed in Table I. It is worth noting that noble gases starting from Ne atom require the same value of $\lambda = 0.5$ and, in general, moving down the periodic table leads to larger optimal values of λ . The mean absolute errors of the srSVWN5—lrGF2 functional, the standard SVWN5 functional, and GF2 are 0.24 eV, 0.26 eV and 0.23 eV, respectively. For the srSVWN5—lrGF2 functional, evaluating IP either from a Green’s function (eq 41) or from the difference between energies of N and $N - 1$ electron systems (eq 35) leads to the same results and these results are converged with respect to the basis set size. In contrast, for GF2, evaluating IP from eq 41 or eq 35 leads to significantly different results. The GF2 IPs calculated from eq 41 have large errors since the cc-pVTZ basis set is not large enough. The IPs calculated from eq 35 benefit from the cancellation of the basis set error. Consequently, the GF2 magnitude of the error that is presented in Table I benefits from fortuitous cancellations of errors. The benefit of using the range separated functional is in the agreement of IP when using both definitions and in avoiding the need of large basis sets. As we observe from Table I, GF2 tends to predict better IPs for atoms while the srSVWN5—lrGF2 functional is more accurate for molecules.

D. Many-electron self-interaction error

The one- and many-electron self-interaction error in approximate density functionals originates from an incomplete cancellation of the spurious electrons self-repulsion by the exchange energy. GF2 includes all the proper exchange and Hartree self-energy diagrams up to the second order and is, therefore, one-electron self-interaction free. We have previously illustrated that GF2 also has a very small two-electron self-interaction error⁵⁴. On the other hand, LDA, is known to have pronounced one- and many-electron self-interaction errors due to a wrong asymptotic decay of the exchange-correlation potential¹¹³. It seems very likely that an application of GF2 for long-range interactions while keeping LDA within the short range would provide an improvement over LDA

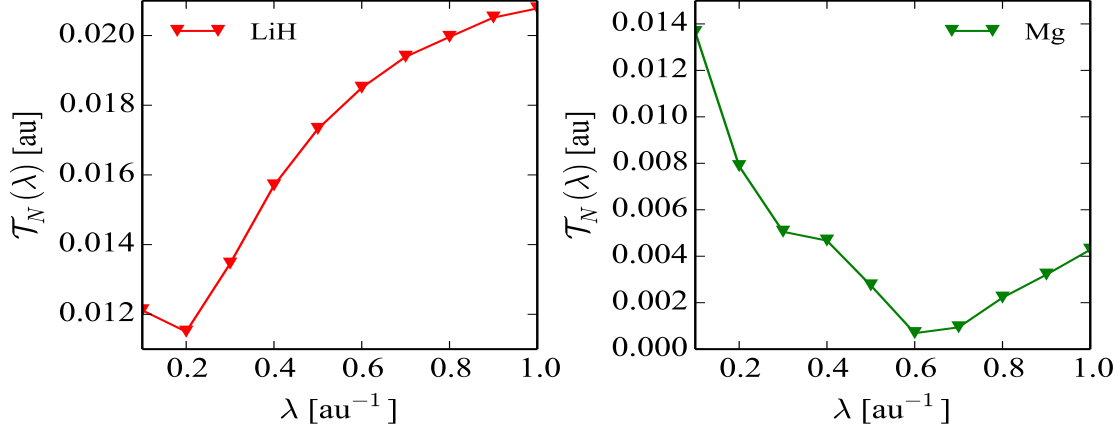


FIG. 5. The absolute difference, as a function of the range separation parameter λ , between IPs calculated from the Green’s function $\mathbf{G}_N^\lambda(\omega)$ and $\text{IP}_{E(N)}^{E(N-1)}$ (from eq 35) using the srSVWN5—lrGF2 functional for LiH molecule (*left panel*) and Mg atom (*right panel*). All calculations were performed in the cc-pVTZ basis set.

TABLE I. Ionization potentials (IP) calculated as $\text{IP} = E_{\text{tot}}(N-1) - E_{\text{tot}}(N)$ using SVWN5, GF2, and srSVWN5—lrGF2 methods. The cc-pVTZ basis set was employed in all calculations. For srSVWN5—lrGF2 calculations, the optimal value of λ is listed in the second column^a.

	Opt.	srSVWN5—lrGF2		GF2		SVWN5		Expt.
	λ	IP	Error	IP	Error	IP	Error	
Atoms								
He	0.9	24.59	0.00	24.36	0.23	24.30	0.29	24.59
Be	0.1	9.17	0.15	8.83	0.49	9.02	0.30	9.32
Ne	0.5	22.16	0.60	21.50	0.06	22.09	0.53	21.56
Mg	0.6	7.52	0.13	7.31	0.34	7.72	0.07	7.65
Ar	0.5	15.97	0.21	15.66	0.10	16.08	0.32	15.76
Ca	0.7	5.98	0.13	5.93	0.18	6.21	0.10	6.11
Kr	0.5	14.33	0.33	14.03	0.03	14.44	0.44	14.00
Molecules								
H ₂ CO	0.1	10.98	0.09	10.86	0.03	10.88	0.01	10.89
CH ₄	0.1	14.29	0.06	14.32	0.03	14.02	0.33	14.35
NH ₃	0.8	10.72	0.10	10.70	0.12	11.01	0.19	10.82
N ₂	0.1	15.66	0.08	15.15	0.43	15.58	0.00	15.58
Li ₂	0.3	5.34	0.61	4.94	0.21	5.31	0.58	4.73
CO ₂	0.1	14.32	0.55	13.88	0.11	13.99	0.22	13.77
CO	0.1	14.14	0.13	13.72	0.29	14.07	0.06	14.01
CH ₃ OH	0.1	10.89	0.07	10.96	0.00	10.76	0.20	10.96
LiH	0.2	8.30	0.40	7.75	0.15	8.21	0.31	7.90
H ₂ O ₂	0.1	11.46	0.24	11.19	0.51	11.40	0.30	11.70
N ₂ H ₄	0.1	9.53	0.55	9.56	0.58	9.41	0.43	8.98
H ₂ S	0.5	10.54	0.04	10.33	0.17	10.63	0.13	10.50
PH ₃	0.6	10.57	0.02	10.47	0.12	10.65	0.06	10.59
HCN	1.2	12.09	0.70	12.90	0.70	14.04	0.44	13.60
Na ₂	0.6	4.94	0.05	4.68	0.21	5.25	0.36	4.89
m.a.v.			0.24		0.23		0.26	

^a Experimental geometries and vertical IPs were taken from NIST Computational Chemistry Comparison and Benchmark Database¹⁰⁸.

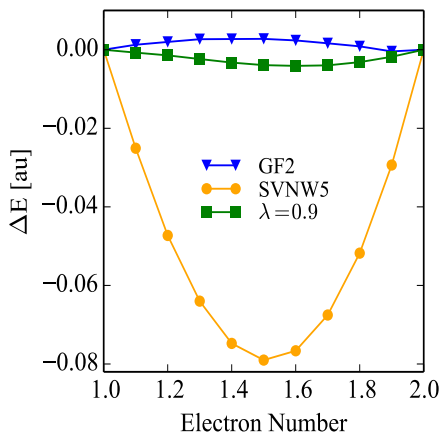


FIG. 6. The energy difference $\Delta E = E^{\mathcal{M}} - E_{\text{lin}}^{\mathcal{M}}$ for He atom, calculated using the srSVWN5—lrGF2 functional with the IP-tuned optimal value of $\lambda = 0.9$ in comparison to that of SVWN5 and GF2 with the aug-cc-pVTZ basis set. $E^{\mathcal{M}}$ is the energy evaluated with a fractional electron number, and $E_{\text{lin}}^{\mathcal{M}}$ is the linear interpolation between integer electron points for method \mathcal{M} .

by itself. In this section, we analyze in detail the self-interaction error of the srSVWN5—lrGF2 functional. As we mentioned earlier, the fractional charge error is directly related to the self-interaction error. To observe it, we calculated the total electronic energy of He atom as a function of the fractional electron number: $N = 1 + \delta$ for $\delta \in [0, 1]$. In Figure 6, we plot the deviation from the linearity: $\Delta E = E^{\mathcal{M}}(N) - E_{\text{lin}}^{\mathcal{M}}$, where $E^{\mathcal{M}}(N)$ is the energy from method \mathcal{M} calculated for a system with N electrons and $E_{\text{lin}}^{\mathcal{M}}$ is the linear interpolation between integer electron points for the same method \mathcal{M} . The IP-tuned optimal value of $\lambda = 0.9$ was used in srSVWN5—lrGF2 calculations. The aug-cc-pVTZ¹¹⁴ basis set was employed in all calculations. It is clear from Figure 6 that GF2 has a very small fractional charge error showing a small concave behavior, therefore indicating a small localization error. SVWN5 exhibits a massive fractional charge error and pronounced convex character. This opposite behavior of SVWN5 indicates a delocalization error common for local, semilocal, and hybrid density functionals¹¹⁵. On the other hand, srSVWN5—lrGF2 calculations for the IP-tuned range separation parameter λ display only a slightly convex behavior and errors that are very similar to GF2, thus greatly improving over SVWN5. We conclude that adding a fraction of the many-body Green’s function method can significantly mitigate the self-interaction error present in the standard density functionals. In this regard, the srSVWN5—lrGF2 functional is similar to popular range-separated hybrid functionals employing the exact exchange for long-range interactions.

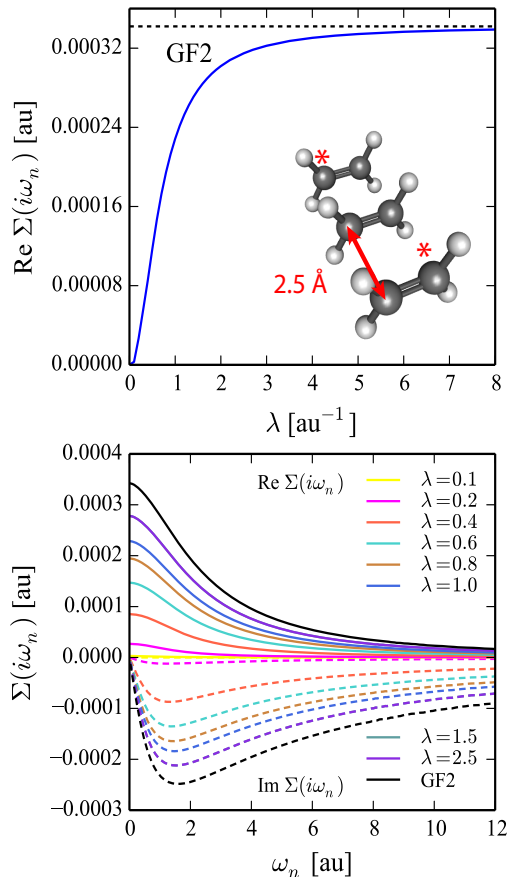


FIG. 7. *Top panel*: The real part of the srSVWN5—lrGF2 self-energy matrix element between two carbon atoms denoted by red stars for the $n = 0$ imaginary frequency as a function of the range separation parameter λ for three ethylene molecules arranged as shown in the inset. *Bottom panel*: Both real (solid lines) and imaginary (dashed lines) parts of the self-energy as a function of the imaginary frequency calculated for different values of λ (bottom). All calculations are with DZP basis set.

E. Locality of self-energy

In this section, we discuss implications of using range-separated hybrid functionals for the self-energy. It is expected that by varying λ the magnitude of self-energy can be gradually changed. To illustrate this, srSVWN5—lrGF2 calculations were performed for three ethylene molecules, each at the experimental geometry¹⁰⁸, placed 2.5 Å apart from each other (see the top panel of Figure 7). A matrix element of the imaginary frequency self-energy between $2p$ orbitals of the two most distant carbon atoms, denoted by red stars on the top panel of Figure 7, is calculated as a function of λ using the DZP¹¹⁶ basis set. Real and imaginary parts of self-energy for different λ values are shown in the bottom panel of Figure 7 using solid and dashed lines, respectively. Colors from the lightest to the darkest correspond to an increasing fraction of GF2. The self-energy increases most rapidly

for small values of λ , up to $\lambda \approx 0.7 - 0.9$, then it begins to slowly converge to the GF2 self-energy. To see it more clearly, in the top panel of Figure 7, we plotted the real part of self-energy for $n = 0$ Matsubara frequency. It grows most rapidly for the small fractions of GF2. Overall this behavior resembles the error function which is used to scale the two-electron integrals to obtain the long-range terms. The possibility to arbitrarily scale the self-energy in the range separated approach has important consequences. For example, the srSVWN5—lrGF2 calculation is less computationally demanding comparing to the standard GF2 calculation since the evaluation of the self-energy according to eq 42 can be carried over a truncated set of orbitals due to the faster decay of its matrix elements. Additionally, using a range-separated Green’s function functional as a low-level method e.g. in self-energy embedding theory^{51–53,117} calculations of periodic systems can be beneficial since, as we demonstrated before, such hybrids require smaller basis sets than the original *ab-initio* Green’s function methods. Consequently, they possibly eliminate many problems such as linear dependences that happen when large, diffuse basis sets are used in calculations of periodic systems. Moreover, using these hybrid approaches, the number of unit cells required to evaluate the self-energy matrix is lowered due to a faster decay of its intercell matrix elements.

V. CONCLUSIONS AND OUTLOOK

In this paper, we have discussed the theoretical framework for building a range-separated hybrid functional combining both DFT and Green’s function methods. In principle, this framework is general and can be used to combine various DFT functionals and Green’s function methods. In particular, to maintain the generality of our discussion, we have focused on describing the relationship of this range-separated functional to the Luttinger-Ward functional which is temperature dependent. Since at present, only the zero temperature DFT functionals are well established, we executed all the practical applications of the short-range DFT – long-range Green’s function functional using the zero temperature SVWN5 functional for the description of the short range and the temperature dependent GF2 method setting $T \rightarrow 0$ for the description of the long range.

We believe that the presented range-separated hybrid functional called srSVWN5—lrGF2 is interesting for two communities. In condensed matter, among the LDA+DMFT practitioners, there has been a long-standing problem of removing the double counting of electron correlation present when LDA is combined with the DMFT treatment employing the Green’s function methods. We believe that our presentation of the short-range DFT – long-range Green’s function functional is directly relevant to this community and gives a rigorous prescription how to avoid the double counting problem by employing the range separation of Coulomb integrals.

Provided that the range separation parameter λ can be optimized based on one of the exact properties of either the DFT or the Green’s function methods, such a range-separated hybrid provides an *ab-initio* treatment of realistic systems.

On the other hand, the short-range DFT – long-range Green’s function hybrid functional is obviously relevant to the DFT community since it can be viewed as a higher rung of the “Jacob’s ladder” of the functionals. Similarly to other high rungs, srSVWN5—lrGF2 employs unoccupied orbitals, is non-local, and has an explicit frequency dependence. Provided that explicitly temperature dependent short-range DFT functionals become established enough, the presented functional can also be made temperature dependent in a straightforward manner.

We have demonstrated that the functional presented in this work offers several attractive advantages when compared to the methods used in its construction. Similarly to range-separated hybrid functionals with other many-body methods such as CI, MP2, CASCF, NEVPT2, CCSD, and RPA, srSVWN5—lrGF2 exhibits a rapid convergence with respect to the one-electron basis set. This fast convergence with respect to the basis set size, for the Green’s function methods provides an additional advantage, since smaller basis sets require fewer imaginary time and imaginary frequency grid points, resulting in reduced computational cost. Additionally, we have illustrated that the srSVWN5—lrGF2 functional has a smaller self-interaction error when compared to the standard SVWN5 functional. This is beneficial in calculations involving molecular thermochemistry, reaction barriers, binding energy in charge transfer complexes, polarizabilities, and molecular conductance. Even though the standard density functionals provide an accurate description of the short-range dynamical correlation, we have shown on the example of the HF and H₂ molecules that the srSVWN5—lrGF2 functional can describe the dynamical correlation even more accurately.

Moreover, we presented a first principles approach to finding an optimal value of the range separation parameter based on the calculation of ionization potentials of atoms and molecules. While the overall accuracy of the IPs evaluated using srSVWN5—lrGF2 is similar to that of GF2 evaluated as the difference between total electronic energies of N and $N - 1$ electron systems, srSVWN5—lrGF2 results are converged with respect to the basis set size and do not rely on any fortuitous cancellation of errors. Moreover, for srSVWN5—lrGF2 evaluating the IP directly from the Green’s function poles or using the energy difference between N and $N - 1$ electron systems results in the same answer. This is not the case for GF2 when the calculations are carried out in a basis set that is not large enough.

We have demonstrated that using the range-separated Coulomb integrals the magnitude of the self-energy in the Green’s function method can be modified as a function of the range separation parameter λ . These results demonstrate that srSVWN5—lrGF2 functional can be useful for

self-energy embedding calculations as well as for Green's function-based calculations of extended systems since for certain values of the parameter λ the decay of self-energy elements is fast and can contribute to an additional sparsity of the problem. Consequently, a fewer number of self-energy elements need to be evaluated resulting in an overall reduction of the computational cost.

Finally, we believe that there are several directions in which short-range DFT with long-range Green's functions hybrid functionals can be further developed. In its current implementation the local density functional describes not only the short-range interactions but also the coupling region between short-range and long-range correlations³⁶. It has been shown⁴⁴ that when the coupling region is treated by many-body methods instead of density functionals, then such a calculation results in a further improvement of functional properties. Therefore, the development of such range-separated double-hybrid functionals¹¹⁸ based on long-range Green's function methods may be worth pursuing.

Another interesting direction for the functional proposed in this work is the study of metallic systems or systems with small band gaps. Green's function expan-

sions that do not include the infinite sum of bubble diagrams such as a Møller–Plesset Green's function are experiencing divergences for metallic systems. These divergences can be efficiently eliminated by screening of the electron-electron interactions provided by e. g. the error function. Therefore, functionals employing a range separation similar to the one presented here, may also be applied to periodic calculations of metallic systems in order to avoid a divergent behavior. Furthermore, several other choices than GF2 such as GW or FLEX are possible as long-range Green's function methods. On the density functional side, it is worth investigating short-range semilocal density functionals within the range separation framework.

VI. ACKNOWLEDGEMENT

A.A.K., and D.Z. acknowledge support from the U.S. Department of Energy (DOE) grant No. ER16391. A.A.K. was also supported by the University of Michigan Rackham Predoctoral Fellowship. A.A.K. is grateful to Dr. Alexander Rusakov for multiple useful discussions.

* akanane@umich.edu

¹ P. Hohenberg and W. Kohn, Phys. Rev. **136**, B864 (1964).

² W. Kohn and L. J. Sham, Phys. Rev. **140**, A1133 (1965).

³ E. Engel and R. Dreizler, *Density Functional Theory: An Advanced Course* (Springer: Berlin, Heidelberg, Germany, 2011) pp 1-224.

⁴ A. Dreuw, J. L. Weisman, and M. Head-Gordon, J. Chem. Phys. **119**, 2943 (2003).

⁵ S. Kristyán and P. Pulay, Chem. Phys. Lett. **229**, 175 (1994).

⁶ D. J. Tozer and N. C. Handy, J. Chem. Phys. **109**, 10180 (1998).

⁷ J. P. Perdew and A. Zunger, Phys. Rev. B **23**, 5048 (1981).

⁸ C. Møller and M. S. Plesset, Phys. Rev. **46**, 618 (1934).

⁹ R. J. Bartlett and M. Musiał, Rev. Mod. Phys. **79**, 291 (2007).

¹⁰ B. Roos, R. Lindh, P. Malmqvist, V. Veryazov, and P. Widmark, *Multiconfigurational Quantum Chemistry* (Wiley & Sons, Inc.: Hoboken, NJ, 2016) pp 103-219.

¹¹ H. Stoll and A. Savin, in *Density functional Methods in Physics*, edited by R. M. Dreizler and J. da Providência (Plenum Press: New York, NY, USA, 1985) pp 177-207.

¹² T. Leininger, H. Stoll, H.-J. Werner, and A. Savin, Chem. Phys. Lett. **275**, 151 (1997).

¹³ J. Toulouse, F. Colonna, and A. Savin, Phys. Rev. A **70**, 062505 (2004).

¹⁴ R. Baer, E. Livshits, and U. Salzner, Annu. Rev. Phys. Chem. **61**, 85 (2010).

¹⁵ T. Yanai, D. P. Tew, and N. C. Handy, Chem. Phys. Lett. **393**, 51 (2004).

¹⁶ J. Heyd, G. E. Scuseria, and M. Ernzerhof, J. Chem. Phys. **118**, 8207 (2003).

¹⁷ H. Iikura, T. Tsuneda, T. Yanai, and K. Hirao, J. Chem. Phys. **115**, 3540 (2001).

¹⁸ J.-D. Chai and M. Head-Gordon, J. Chem. Phys. **128**, 084106 (2008).

¹⁹ O. A. Vydrov and G. E. Scuseria, J. Chem. Phys. **125**, 234109 (2006).

²⁰ Y. Tawada, T. Tsuneda, S. Yanagisawa, T. Yanai, and K. Hirao, J. Chem. Phys. **120**, 8425 (2004).

²¹ M. J. G. Peach, T. Helgaker, P. Salek, T. W. Keal, O. B. Lutnaes, D. J. Tozer, and N. C. Handy, Phys. Chem. Chem. Phys. **8**, 558 (2006).

²² J. G. Ángyán, I. C. Gerber, A. Savin, and J. Toulouse, Phys. Rev. A **72**, 012510 (2005).

²³ E. Fromager and H. J. A. Jensen, Phys. Rev. A **78**, 022504 (2008).

²⁴ O. Kullie and T. Saue, Chem. Phys. **395**, 54 (2012).

²⁵ J. G. Ángyán, Phys. Rev. A **78**, 022510 (2008).

²⁶ E. Fromager, R. Cimraglia, and H. J. A. Jensen, Phys. Rev. A **81**, 024502 (2010).

²⁷ E. Goll, H.-J. Werner, and H. Stoll, Phys. Chem. Chem. Phys. **7**, 3917 (2005).

²⁸ B. G. Janesko, T. M. Henderson, and G. E. Scuseria, J. Chem. Phys. **130**, 081105 (2009).

²⁹ J. Toulouse, I. C. Gerber, G. Jansen, A. Savin, and J. G. Ángyán, Phys. Rev. Lett. **102**, 096404 (2009).

³⁰ J. Toulouse, W. Zhu, J. G. Ángyán, and A. Savin, Phys. Rev. A **82**, 032502 (2010).

³¹ R. Pollet, A. Savin, T. Leininger, and H. Stoll, J. Chem. Phys. **116**, 1250 (2002).

³² E. Fromager, F. Réal, P. Wählin, U. Wahlgren, and H. J. A. Jensen, J. Chem. Phys. **131**, 054107 (2009).

³³ E. Fromager, J. Toulouse, and H. J. A. Jensen, J. Chem. Phys. **126**, 074111 (2007).

³⁴ K. Pernal, Phys. Rev. A **81**, 052511 (2010).

³⁵ D. R. Rohr, J. Toulouse, and K. Pernal, Phys. Rev. A **82**, 052502 (2010).

- ³⁶ J. Toulouse, A. Savin, and H.-J. Flad, *Int. J. Quantum Chem.* **100**, 1047 (2004).
- ³⁷ P. Gori-Giorgi and A. Savin, *Phys. Rev. A* **73**, 032506 (2006).
- ³⁸ I. C. Gerber and J. G. Ángyán, *Chem. Phys. Lett.* **416**, 370 (2005).
- ³⁹ R.-F. Liu, C. A. Franzese, R. Malek, P. S. Żuchowski, J. G. Ángyán, M. M. Szcześniak, and G. Chalaśiński, *J. Chem. Theory Comput.* **7**, 2399 (2011).
- ⁴⁰ W. Zhu, J. Toulouse, A. Savin, and J. G. Ángyán, *J. Chem. Phys.* **132**, 244108 (2010).
- ⁴¹ J. Paier, B. G. Janesko, T. M. Henderson, G. E. Scuseria, A. Grüneis, and G. Kresse, *J. Chem. Phys.* **132**, 094103 (2010).
- ⁴² O. Franck, B. Mussard, E. Luppi, and J. Toulouse, *J. Chem. Phys.* **142**, 074107 (2015).
- ⁴³ B. G. Janesko and G. E. Scuseria, *Phys. Chem. Chem. Phys.* **11**, 9677 (2009).
- ⁴⁴ Y. Cornaton, A. Stoyanova, H. J. A. Jensen, and E. Fromager, *Phys. Rev. A* **88**, 022516 (2013).
- ⁴⁵ B. G. Janesko, T. M. Henderson, and G. E. Scuseria, *J. Chem. Phys.* **131**, 034110 (2009).
- ⁴⁶ R. M. Irelan, T. M. Henderson, and G. E. Scuseria, *J. Chem. Phys.* **135**, 094105 (2011).
- ⁴⁷ A. L. Fetter and J. D. Walecka, *Quantum Theory of Many-Particle Systems* (Dover Publications: Mineola, NY, USA, 2003) pp 64-83.
- ⁴⁸ G. Stefanucci and R. van Leeuwen, *Nonequilibrium Many-Body Theory of Quantum Systems: A Modern Introduction* (Cambridge University Press: Cambridge, UK, 2013) pp 249-323.
- ⁴⁹ A. Abrikosov, L. Gorkov, and I. E. Dzyaloshinski, *Methods of Quantum Field Theory in Statistical Physics* (Dover Publications, Inc.: New York, USA, 1963) pp 97-200.
- ⁵⁰ J. J. Phillips and D. Zgid, *J. Chem. Phys.* **140**, 241101 (2014).
- ⁵¹ A. A. Kananenka, E. Gull, and D. Zgid, *Phys. Rev. B* **91**, 121111 (2015).
- ⁵² T. N. Lan, A. A. Kananenka, and D. Zgid, *J. Chem. Phys.* **143**, 241102 (2015).
- ⁵³ T. N. Lan and D. Zgid, *J. Phys. Chem. Lett.* **8**, 2200 (2017).
- ⁵⁴ J. J. Phillips, A. A. Kananenka, and D. Zgid, *J. Chem. Phys.* **142**, 194108 (2015).
- ⁵⁵ P. A. M. Dirac, *Math. Proc. Cambridge Philos. Soc.* **26**, 376 (1930).
- ⁵⁶ S. H. Vosko, L. Wilk, and M. Nusair, *Can. J. Phys.* **58**, 1200 (1980).
- ⁵⁷ L. J. Holleboom and J. G. Snijders, *J. Chem. Phys.* **93**, 5826 (1990).
- ⁵⁸ N. E. Dahlen and R. van Leeuwen, *J. Chem. Phys.* **122**, 164102 (2005).
- ⁵⁹ P. Mori-Sánchez, A. J. Cohen, and W. Yang, *Phys. Rev. A* **85**, 042507 (2012).
- ⁶⁰ G. Kotliar, S. Y. Savrasov, K. Haule, V. S. Oudovenko, O. Parcollet, and C. A. Marianetti, *Rev. Mod. Phys.* **78**, 865 (2006).
- ⁶¹ A. Georges and G. Kotliar, *Phys. Rev. B* **45**, 6479 (1992).
- ⁶² J. Lee and K. Haule, *Phys. Rev. B* **91**, 155144 (2015).
- ⁶³ V. I. Anisimov, F. Aryasetiawan, and A. I. Lichtenstein, *J. Phys. Cond. Mat.* **9**, 767 (1997).
- ⁶⁴ K. Haule, C.-H. Yee, and K. Kim, *Phys. Rev. B* **81**, 195107 (2010).
- ⁶⁵ M. A. Rohrdanz and J. M. Herbert, *J. Chem. Phys.* **129**, 034107 (2008).
- ⁶⁶ T. Stein, H. Eisenberg, L. Kronik, and R. Baer, *Phys. Rev. Lett.* **105**, 266802 (2010).
- ⁶⁷ T. Körzdörfer, J. S. Sears, C. Sutton, and J.-L. Brédas, *J. Chem. Phys.* **135**, 204107 (2011).
- ⁶⁸ E. Livshits and R. Baer, *Phys. Chem. Chem. Phys.* **9**, 2932 (2007).
- ⁶⁹ J.-W. Song, T. Hirose, T. Tsuneda, and K. Hirao, *J. Chem. Phys.* **126**, 154105 (2007).
- ⁷⁰ M. Levy, *Proc. Natl. Acad. Sci. U.S.A.* **76**, 6062 (1979).
- ⁷¹ J. Harris and R. O. Jones, *J. Phys. F: Met. Phys.* **4**, 1170 (1974).
- ⁷² O. Gunnarsson and B. I. Lundqvist, *Phys. Rev. B* **13**, 4274 (1976).
- ⁷³ D. C. Langreth and J. P. Perdew, *Phys. Rev. B* **15**, 2884 (1977).
- ⁷⁴ J. Harris, *Phys. Rev. A* **29**, 1648 (1984).
- ⁷⁵ J. P. Dombroski, S. W. Taylor, and P. M. W. Gill, *J. Phys. Chem.* **100**, 6272 (1996).
- ⁷⁶ P. M. W. Gill, R. D. Adamson, and J. A. Pople, *Mol. Phys.* **88**, 1005 (1996).
- ⁷⁷ J. P. Perdew and Y. Wang, *Phys. Rev. B* **45**, 13244 (1992).
- ⁷⁸ A. Seidl, A. Görling, P. Vogl, J. A. Majewski, and M. Levy, *Phys. Rev. B* **53**, 3764 (1996).
- ⁷⁹ R. Jishi, *Feynman Diagram Techniques in Condensed Matter Physics* (Cambridge University Press: Cambridge, UK, 2014) pp 179-210.
- ⁸⁰ L. Hedin, *Phys. Rev.* **139**, A796 (1965).
- ⁸¹ F. Aryasetiawan and O. Gunnarsson, *Rep. Prog. Phys.* **61**, 237 (1998).
- ⁸² N. E. Bickers, D. J. Scalapino, and S. R. White, *Phys. Rev. Lett.* **62**, 961 (1989).
- ⁸³ N. Bickers and D. Scalapino, *Ann. Phys.* **193**, 206 (1989).
- ⁸⁴ G. Baym and L. P. Kadanoff, *Phys. Rev.* **124**, 287 (1961).
- ⁸⁵ G. Baym, *Phys. Rev.* **127**, 1391 (1962).
- ⁸⁶ Y. Lu, M. Höppner, O. Gunnarsson, and M. W. Haverkort, *Phys. Rev. B* **90**, 085102 (2014).
- ⁸⁷ D. V. Neck, K. Peirs, and M. Waroquier, *J. Chem. Phys.* **115**, 15 (2001).
- ⁸⁸ K. Peirs, D. V. Neck, and M. Waroquier, *J. Chem. Phys.* **117**, 4095 (2002).
- ⁸⁹ T. Matsubara, *Prog. Theor. Phys.* **14**, 351 (1955).
- ⁹⁰ V. M. Galitskii and A. B. Migdal, *J. Exptl. Theoret. Phys.* **34**, 139 (1958).
- ⁹¹ J. M. Luttinger and J. C. Ward, *Phys. Rev.* **118**, 1417 (1960).
- ⁹² D. W. Smith and O. W. Day, *J. Chem. Phys.* **62**, 113 (1975).
- ⁹³ O. W. Day, D. W. Smith, and R. C. Morrison, *J. Chem. Phys.* **62**, 115 (1975).
- ⁹⁴ J. M. O. Matos and O. W. Day, *Int. J. Quantum Chem.* **31**, 871 (1987).
- ⁹⁵ R. C. Morrison, *J. Chem. Phys.* **96**, 3718 (1992).
- ⁹⁶ A. Szabo and N. Ostlund, *Modern Quantum Chemistry: Introduction to Advanced Electronic Structure Theory* (McGraw-Hill, Inc.: USA, 1989) pp 389-392.
- ⁹⁷ J. P. Perdew, R. G. Parr, M. Levy, and J. L. Balduz, *Phys. Rev. Lett.* **49**, 1691 (1982).
- ⁹⁸ J. P. Perdew, A. Ruzsinszky, G. I. Csonka, O. A. Vydrov, G. E. Scuseria, V. N. Staroverov, and J. Tao, *Phys. Rev. A* **76**, 040501 (2007).

- ⁹⁹ P. Mori-Sánchez, A. J. Cohen, and W. Yang, *J. Chem. Phys.* **125**, 201102 (2006).
- ¹⁰⁰ K. Aidas, C. Angeli, K. L. Bak, V. Bakken, R. Bast, L. Boman, O. Christiansen, R. Cimiraglia, S. Coriani, P. Dahle, E. K. Dalskov, U. Ekström, T. Enevoldsen, J. J. Eriksen, P. Ettenhuber, B. Fernández, L. Ferrighi, H. Fliegl, L. Frediani, K. Hald, A. Halkier, C. Hättig, H. Heiberg, T. Helgaker, A. C. Hennum, H. Hettema, E. Hjertenæs, S. Høst, I.-M. Høyvik, M. F. Iozzi, B. Jansík, H. J. Aa. Jensen, D. Jonsson, P. Jørgensen, J. Kauczor, S. Kirpekar, T. Kjærgaard, W. Klopper, S. Knecht, R. Kobayashi, H. Koch, J. Kongsted, A. Krapp, K. Kristensen, A. Ligabue, O. B. Lutnæs, J. I. Melo, K. V. Mikkelsen, R. H. Myhre, C. Neiss, C. B. Nielsen, P. Norman, J. Olsen, J. M. H. Olsen, A. Osted, M. J. Packer, F. Pawłowski, T. B. Pedersen, P. F. Provasi, S. Reine, Z. Rinkevicius, T. A. Ruden, K. Ruud, V. V. Rybkin, P. Salek, C. C. M. Samson, A. S. de Merás, T. Saue, S. P. A. Sauer, B. Schimmelpfennig, K. Sneskov, A. H. Steindal, K. O. Sylvester-Hvid, P. R. Taylor, A. M. Teale, E. I. Tellgren, D. P. Tew, A. J. Thorvaldsen, L. Thøgersen, O. Vahtras, M. A. Watson, D. J. D. Wilson, M. Ziolkowski, and H. Ågren, *Wiley Interdiscip. Rev. Comput. Mol. Sci.* **4**, 269 (2014).
- ¹⁰¹ A. A. Kananenka, J. J. Phillips, and D. Zgid, *J. Chem. Theory Comput.* **12**, 564 (2016).
- ¹⁰² A. A. Kananenka, A. R. Welden, T. N. Lan, E. Gull, and D. Zgid, *J. Chem. Theory Comput.* **12**, 2250 (2016).
- ¹⁰³ M. J. Frisch, G. W. Trucks, H. B. Schlegel, G. E. Scuseria, M. A. Robb, J. R. Cheeseman, G. Scalmani, V. Barone, B. Mennucci, G. A. Petersson, H. Nakatsuji, M. Caricato, X. Li, H. P. Hratchian, A. F. Izmaylov, J. Bloino, G. Zheng, J. L. Sonnenberg, M. Hada, M. Ehara, K. Toyota, R. Fukuda, J. Hasegawa, M. Ishida, T. Nakajima, Y. Honda, O. Kitao, H. Nakai, T. Vreven, J. A. Montgomery, Jr., J. E. Peralta, F. Ogliaro, M. Bearpark, J. J. Heyd, E. Brothers, K. N. Kudin, V. N. Staroverov, R. Kobayashi, J. Normand, K. Raghavachari, A. Rendell, J. C. Burant, S. S. Iyengar, J. Tomasi, M. Cossi, N. Rega, J. M. Millam, M. Klene, J. E. Knox, J. B. Cross, V. Bakken, C. Adamo, J. Jaramillo, R. Gomperts, R. E. Stratmann, O. Yazyev, A. J. Austin, R. Cammi, C. Pomelli, J. W. Ochterski, R. L. Martin, K. Morokuma, V. G. Zakrzewski, G. A. Voth, P. Salvador, J. J. Dannenberg, S. Dapprich, A. D. Daniels, Ö. Farkas, J. B. Foresman, J. V. Ortiz, J. Cioslowski, and D. J. Fox, "Gaussian09 Revision A.01," Gaussian, Inc., Wallingford, CT, 2009.
- ¹⁰⁴ T. H. J. Dunning, *J. Chem. Phys.* **90**, 1007 (1989).
- ¹⁰⁵ D. E. Woon and T. H. Dunning, *J. Chem. Phys.* **100**, 2975 (1994).
- ¹⁰⁶ B. P. Prascher, D. E. Woon, K. A. Peterson, T. H. Dunning, and A. K. Wilson, *Theor. Chem. Acc.* **128**, 69 (2011).
- ¹⁰⁷ K. Raghavachari, G. W. Trucks, J. A. Pople, and M. Head-Gordon, *Chem. Phys. Lett.* **157**, 479 (1989).
- ¹⁰⁸ R. D. Johnson, "NIST Computational Chemistry Comparison and Benchmark Database," Standard Reference Database Number 101 Release 16a, NIST: Gaithersburg, MD, 2013, (accessed May 15, 2017).
- ¹⁰⁹ A. K. Wilson, D. E. Woon, K. A. Peterson, and T. H. D. Jr., *J. Chem. Phys.* **110**, 7667 (1999).
- ¹¹⁰ D. E. Woon and T. H. Dunning, *J. Chem. Phys.* **98**, 1358 (1993).
- ¹¹¹ J. Koput and K. A. Peterson, *J. Phys. Chem. A* **106**, 9595 (2002).
- ¹¹² R. Burden and J. Faires, *Numerical analysis* (Brooks/Cole, Cengage Learning: Boston, MA, USA, 2010) pp 48-56.
- ¹¹³ R. van Leeuwen and E. J. Baerends, *Phys. Rev. A* **49**, 2421 (1994).
- ¹¹⁴ D. E. Woon and T. H. Dunning, *J. Chem. Phys.* **100**, 2975 (1994).
- ¹¹⁵ A. J. Cohen, P. Mori-Sánchez, and W. Yang, *Chem. Rev.* **112**, 289 (2012).
- ¹¹⁶ T. H. Dunning, *J. Chem. Phys.* **53**, 2823 (1970).
- ¹¹⁷ T. N. Lan, A. A. Kananenka, and D. Zgid, *J. Chem. Theory Comput.* **12**, 4856 (2016).
- ¹¹⁸ J. Toulouse, P. Gori-Giorgi, and A. Savin, *Theor. Chem. Acc.* **114**, 305 (2005).